Monthly Notices of the ROYAL ASTRONOMICAL SOCIETY

MNRAS **523,** 5502–5509 (2023) https://doi.org/10.1093/mnras/stad1774
Advance Access publication 2023 June 14

A decade of near-infrared variability in NGC4388: insights into the AGN structure

Luis G. Dahmer-Hahn,[1]★ Alberto Rodríguez-Ardila,[2,3]★ Marina Bianchin,[4,5] Rogemar A. Riffel,[4] Rogério Riffel,[6,7] Thaisa Storchi-Bergmann[6] and Lei Hao[1]

[1]*Key Laboratory for Research in Galaxies and Cosmology, Shanghai Astronomical Observatory, Chinese Academy of Sciences, 80 Nandan Road, Shanghai 200030, China*
[2]*Laboratório Nacional de Astrofísica, Rua dos Estados Unidos, 154, Itajubá 37504-364, MG, Brazil*
[3]*Instituto Nacional de Pesquisas Espaciais, Av. dos Astronautas, 1758 – Jardim da Granja, São José dos Campos, SP 12227-010, Brazil*
[4]*Departamento de Física, Centro de Ciências Naturais e Exatas, Universidade Federal de Santa Maria, Santa Maria 97105-900, RS, Brazil*
[5]*Department of Physics and Astronomy, University of California, 4129 Frederick Reines Hall, Irvine, CA 92697, USA*
[6]*Instituto de Física, Universidade Federal do Rio Grande do Sul, Av. Bento Gonçalves, Porto Alegre 9500, 91501-970, RS, Brazil*
[7]*Instituto de Astrofísica de Canarias, E-38200 La Laguna, Tenerife, Spain*

Accepted 2023 June 9. Received 2023 June 8; in original form 2023 April 30

ABSTRACT

Variability studies have proven to be a powerful diagnostic tool for understanding the physics and properties of active galactic nuclei (AGNs). They provide insights into the spatial and temporal distribution of the emitting regions, the structure and dynamics of the accretion disc, and the properties of the central black hole. Here, we have analysed the *K*-band spectral variability of the Seyfert 1.9/2 galaxy NGC 4388 spanning five epochs over a period of 10 yr. We have performed spectral synthesis of the nuclear region and found that the contribution of warm dust ($T \sim 800$ K) declined by 88 per cent during these 10 yr. In the same period, the [Ca VIII] coronal line decreased 61 per cent, whereas Br γ emission declined 35 per cent. For the He I and H_2, we did not detect any significant variation beyond their uncertainties. Based on the time span of these changes, we estimate that the region where the warm dust is produced is smaller than 0.6 pc, which suggests that this spectral feature comes from the innermost part of the region sampled, directly from the AGN torus. On the other hand, the bulk of [Ca VIII] is produced in the inner ∼2 pc and the nuclear Br γ region is more extended, spanning a region larger than 3 pc. Lastly, He I and H_2 are even more external, with most of the emission probably being produced in the host galaxy rather than in the AGN. This is the first spectroscopic variability study in the near-infrared for an AGN where the central source is not directly visible.

Key words: galaxies: active – galaxies: individual: NGC 4388 – galaxies: nuclei – galaxies: Seyfert – galaxies: spiral.

1 INTRODUCTION

Active galactic nuclei (AGNs) are among the most energetic and luminous objects in the Universe, reaching integrated luminosities of up to 10^{48} erg s^{-1} (Koratkar & Blaes 1999; Bischetti et al. 2017). They are powered by the accretion of matter on to supermassive black holes (SMBHs) at their centres, which can release huge amounts of energy across the electromagnetic spectrum (e.g. Netzer 2015; Padovani et al. 2017; Storchi-Bergmann & Schnorr-Müller 2019). AGNs display a wide range of observational properties, including broad emission lines, continuum radiation spanning a broad range of wavelengths, and often exhibit variability on different time-scales (Peterson 2001; Gaskell & Klimek 2003; Padovani et al. 2017).

AGNs have been found to be variable at all wavelengths at which they have been observed (Peterson 2001), from γ-rays (e.g. Gaidos et al. 1996) and X-rays (e.g. McHardy 2001; Sanfrutos et al. 2016; Mehdipour et al. 2017), going through visible light (Winge et al. 1995, 1996; Burke et al. 2021), up to longer wavelengths such as infrared (e.g. Koshida et al. 2014; Sánchez et al. 2017) and radio (e.g. Hovatta et al. 2007). Depending on the properties of the AGN, this variability can happen in very different time-scales, ranging from minutes to decades, with different time-scales and wavelength ranges being attributed to different physical processes.

Variability studies in AGNs have been essential for advancing our understanding of the physical processes that occur in these objects. For example, studies of AGN variability have been used to probe the structure and dynamics of the accretion disc. They have also been used to investigate the mass and spin of the central black hole (e.g. McHardy et al. 2006; Cackett et al. 2013; Emmanoulopoulos et al. 2014; McHardy et al. 2014).

It is expected that the variability of the central source will leave fingerprints on high-ionization emission lines, such as the coronal lines, as well as on the hot dust emission from the clumpy torus, since they are directly associated with the AGN emission. Despite offering insight into so many interesting features, variability studies on the near-infrared (NIR) are rare. Koshida et al. (2014) presented a dust reverberation survey for 17 nearby Seyfert 1 galaxies. They found a delayed response of the *K*-band light curve after the *V*-band light curve ranging between 9 and 170 d for all targets. They also found

★ E-mail: luisgdh@gmail.com (LGD-H); aardila@lna.br (AR-A)

that these lag times strongly correlate with their optical luminosity. However, photometric surveys such as these are technically limited, since they cannot distinguish between emission lines and continuum emission. This distinction gives us insights into the geometry of the central source, as well as into parameters such as flux and dust temperature.

In their study, Sánchez et al. (2017) analysed the photometric NIR light curves of more than 2000 sources within a 1.5 deg^2 area. Over a period of 5 yr, they discovered that AGNs that exhibit broad lines (BL) have a significantly higher proportion of variable sources compared to those with only narrow lines (NL). The authors also found that most of the low-luminosity variable NL sources are likely BL AGN, where the variability signal may be weakened by the host galaxy. In contrast, for high-luminosity variable NL, the authors suggested that these could be examples of true type II AGN or BL AGN with limited spectral coverage, which may result in the BL emission being missed.

So far, NIR spectroscopic reverberation mapping campaigns have been conducted in only two Seyfert 1 galaxies, NGC 5548 (Landt et al. 2019) and Mrk 876 (Landt et al. 2023). For NGC 5548, the authors reported that both the accretion disc and the hot dust contribute to the variability, with lag times of ∼70 d. Also, for Mrk 876, they found that the luminosity-based dust radii are larger than the dust response time obtained by a contemporaneous photometric reverberation mapping campaign, by a factor of ∼2. This result is well explained by a flared, disc-like structure for the hot dust. In both cases, the authors detected dust emission components with temperatures ranging from 1000 to 1500 K.

Such variability studies in AGNs are powerful diagnostic tools for understanding the physics and properties of these objects, providing insights into the spatial and temporal distribution of the emitting regions, the structure and dynamics of the accretion disc, and the properties of the central black hole. Thus, variable AGNs are key to the understanding of geometrical properties of the inner region.

Generally speaking, the more luminous the AGN, the more dramatic its variability can be (Peterson 2001). The main reason for this is that in more luminous sources we have access to smaller and more internal regions, which can vary more easily than bigger and more external areas. Also, it is easier to identify the variability in highly luminous sources. This makes variable, but not-so-bright AGNs (such as Seyfert 2) rare but very important when probing the physics of the circumnuclear regions.

1.1 NGC 4388

NGC 4388 is an SA(s)b galaxy in the constellation of Virgo (Veilleux, Bland-Hawthorn & Cecil 1999), at a distance of 19 Mpc (Kuo et al. 2011). It is one of the brightest galaxies of the Virgo cluster due to its Seyfert 1.9/2 nucleus (Forster, Leighly & Kay 1999). Also, it is nearly edge-on, with an inclination of 79° (Damas-Segovia et al. 2016).

The interstellar medium of the galaxy has undergone a ram pressure stripping event ∼200 Myr ago, leading to a recent quenching of the star formation activity in the outer, gas-free galactic disc (Damas-Segovia et al. 2016; Vollmer et al. 2018). Due to its highly eccentric orbit within the Virgo cluster, the galaxy passed close to the cluster centre, which led to the loss of much of its neutral hydrogen caused by the interaction with the intercluster medium.

Because of its water maser emission from a circumnuclear disc, the mass of its SMBH can be accurately measured. Kuo et al. (2011) studied the kinematics of this water maser by employing very long baseline interferometry, also deriving an SMBH mass of $8.5 \pm 0.2 \times 10^6\,M_\odot$.

Ionized gas extending up to 35 kpc has been found around the galaxy (Yoshida et al. 2002). The same authors reported that the [O III]/Hα map indicates that the inner 12 kpc may be excited by AGN radiation. Also, although the excitation mechanism of the outer region is unclear, it is likely that the nuclear radiation is also a dominant source of its ionization.

This galaxy also has a double-peaked radio jet (Stone, Wilson & Ward 1988; Hummel & Saikia 1991), with a primary peak on the nucleus and a secondary peak 230 pc south-west of it. The same authors also reported the detection of a plume of radio plasma to the north of its nucleus.

In the NIR, this target exhibits complex spatially extended emission lines. According to Rodríguez-Ardila et al. (2017), who analysed this object through NIR spectroscopy, radiation from the central source alone cannot explain the observed high-ionization lines. The additional excitation most likely comes from shocks between the radio jet and the ambient gas.

This source also shows X-ray variability properties. Fedorova et al. (2011) monitored this source between 2003 and 2009 using *INTEGRAL* and *Swift* data, and found slow strong variations of the hard X-ray emission. According to their analysis, the flux variability on time-scales of 3–6 months in the 20–60 keV energy range is of the order of ∼2. They also detected significant spectral shape changes of the 20–300 keV spectrum, uncorrelated with the flux level. Lastly, they found that the lower value of the exponential cut-off at high energies is similar to that of radio-loud AGN, even though NGC 4388 is a radio-quiet object.

All of the above makes this galaxy an ideal target to study AGN properties. As a galaxy with confirmed variability, we are able to assess the geometrical properties of its AGN. Also, since its central source is not directly accessible in the NIR, we are able to probe its circumnuclear properties without the BL region overshadowing the more extended regions.

In this paper, we investigate the variability of this target in the NIR by employing spectroscopic data obtained spanning a period of 10 yr. This paper is structured as follows: In Section 2, we discuss observation and reduction of our data. In Section 3, we discuss the variability at the continuum level. In Section 4, we discuss the variability of the emission lines and in Section 5, we summarize our results and give our final remarks.

2 DATA

Our data contain three cross-dispersed (XD) spectra obtained with: (i) Gemini Near-Infrared Spectrograph (GNIRS; Elias et al. 2006a, b) on the Gemini North 8.1 m telescope; (ii) TripleSpec4 (Vacca, Cushing & Rayner 2003; Cushing, Vacca & Rayner 2004) mounted on the 4-m Víctor M. Blanco Telescope, and (iii) TripleSpec4 on the 4.1-m Southern Astrophysical Research (SOAR) telescope. We also use integral field unit datacubes obtained with the Spectrograph for INtegral Field Observations in the Near Infrared (SINFONI; Bonnet et al. 2003) attached to UT 4, one of the 8-m telescopes of the Very Large Telescope (VLT), and with the Near-Infrared Integral Field Spectrograph (NIFS; McGregor et al. 2003) fed by the Gemini North Adaptive Optics system. A summary of the observations is made in Table 1.

For each data set, an A0V star was observed immediately after or before the galaxy, with similar airmass, in order to flux calibrate as well as correct for telluric absorptions. Data reduction was performed using standard reduction scripts for each instrument. These scripts

Table 1. Main properties of each data set.[1] Observed with adaptive optics, and degraded to 0.6 arcsec.

Date observed	Instrument	Telescope	Seeing (arcmin)	Area	Orientation (°E of N)
2011-04-12	SINFONI	VLT	0.64	IFU	N/A
2013-02-04	GNIRS	Gemini	0.49	0.3 arcsec × 0.3 arcsec	64
2015-07-06	NIFS	Gemini	0.14 [1]	IFU	N/A
2017-04-10	TripleSpec4	Blanco	2.5	1.1 arcsec × 0.6 arcsec	24
2021-06-28	TripleSpec4	SOAR	0.80	1.1 arcsec × 0.6 arcsec	25

consist of the preparation of the data, flat-field correction, wavelength calibration, telluric atmospheric absorption correction, and flux calibration. For integral field units (IFU), these steps also include spatial calibration and 3D datacube construction.

Since longslit spectra have different slit widths and orientations, we performed two extractions to each IFU, by matching cross-dispersed integrated region. Thus, we created two data sets: one with 0.3 arcsec × 0.3 arcsec (covering the yr of 2011, 2013, and 2015; hereafter 0.3 arcsec data set) and one with 1.1 arcsec × 0.6 arcsec (covering the yr of 2011, 2015, 2017, and 2021; hereafter 0.6 arcsec data set). Also, since NIFS datacube was observed with the adaptive optics, we degraded its spatial resolution to 0.6 arcsec before extracting its spectra. Table 1 shows the dates of observation, as well as the instruments, telescopes, and atmospheric conditions.

Since our data set covers different wavelength ranges, in order to avoid any biases, all analyses conducted throughout this paper are limited between 20 000 to 24 000 Å spectral region, since this is the only wavelength range in common in all data sets. It is worth noting that for XD spectra that extend beyond this region (e.g. covering the bluer spectral region 9000–20000 Å), we also performed the same analysis using the data over the full spectral region, and found no differences beyond our error margin compared to the results presented in this paper. The only significant differences occur in the composition of the stellar population vectors, which we do not present nor discuss.

Except for the NIFS datacube, all data were observed on non-photometric nights, and thus their flux calibration relative to each other does not match. Because of that, in order to have a better relative flux calibration, we assumed the NIFS datacube as the correct one. For the remaining data sets, we extracted circular regions centred 1.0 arcsec away from the nucleus, where the AGN emission is negligible, and then scaled it to their corresponding NIFS flux. This scaling was always performed at λ22780, since it is far from prominent stellar absorptions as well as emission lines. In the left-hand panel of Fig. 1, we show the seven spectra used in our analysis. In the upper panels, we show the 0.3 arcsec data set, and in the bottom panel we show the 0.6 arcsec data set. Also, in the left-hand panels we show two representative spectra and their corresponded spectra as modelled by STARLIGHT.

Both SINFONI and GNIRS data suffered from poor Brγ subtraction in their respective telluric stars, resulting in spurious data in the datacubes around Brγ. These regions were masked in our analysis. Also, the NIFS datacube suffers from poor subtraction of sky emission lines, which were also masked during our analysis. None of these issues proved to have any significant impact on our analysis, as they were far enough from the emission lines and did not cover much of the continuum region.

3 CONTINUUM VARIABILITY

In order to disentangle the continuum components, we have followed Riffel et al. (2009) and performed stellar population synthesis using the STARLIGHT code (Cid Fernandes et al. 2004, 2005). We fed the code with the new generation of the X-shooter Spectral Library of simple stellar population (SSP) models (Verro et al. 2022), created with a Kroupa (2001) initial mass function, and PARSEC–COLIBRI isochrones (Bressan et al. 2012; Marigo et al. 2013). We limited the library to the nine most representative ages[1] and four most representative metallicities[2], totalling 36 SSPs. It is worth mentioning that we have degraded the spectral resolution of the models in order to match that of the data. We also added blackbody functions (BB) corresponding to temperatures of 700, 800, 1000, 1200, and 1400 K, and a featureless continuum (FC) with $f_\lambda \propto \lambda^{-0.5}$. For a more detailed description of the code and the method of spectral synthesis for NIR data, see Riffel et al. (2009, 2022). In order to show the quality of the fits, we show in the right-hand panels of Fig. 1 for each data set two spectra with their corresponding synthesis results using STARLIGHT (black). The most prominent emission lines are highlighted in yellow.

We divided black bodies into warm (BB_W, $T \leq 1000$ K) and hot (BB_H, $T > 1000$ K). Since our wavelength range is very narrow and excludes J and H bands, where many important stellar absorptions are located, we combined all SSPs in one group, that we have called StPop group. The synthesis results are presented in Table 2, for the per cent light contribution at 22 780 Å. These same results are presented in Fig. 2, where we show error bars based on upper limits from Cid Fernandes et al. (2014). In this paper, the authors estimated STARLIGHT uncertainties of up to 9 per cent, by inducing σ-level errors on a data set.

We can see from Table 2 and Fig. 2 that along the monitored period, both hot dust and featureless continuum contributions are negligible in this wavelength range, being lower than our errors in all cases. However, these results also show that between 2011 and 2021 the per cent contribution of warm dust decreased by a factor of 2.9 (from 74 per cent to 25 per cent) at the 0.6 arcsec data set, whereas the contribution of stellar population increased by a factor of 3 (from 68 per cent to 23 per cent).

In terms of absolute flux at 22 780 Å, the BB_W contribution decreased from 4.27×10^{-16} to 0.49×10^{-16} erg s^{-1} cm^{-2} Å^{-1} between 2011–2004 and 2021–2006 in the 0.6 arcsec data set, normalized at 22 780 Å. This corresponds to an absolute flux decrease of ∼88 per cent. In the same period, the stellar population flux did not vary beyond our error margin.

In order to better illustrate this change, we measured the radial profile of the continuum at 22 780 Å, using a wavelength window of 100 Å, for the two data sets. These results are presented in Fig. 3. For SINFONI and NIFS datacubes, we simulated slits with orientations of 64 and 25°E of N for the 0.3 and 0.6 arcsec data sets, respectively. Also, since each instrument has different spaxel size, we normalized all radial profiles to the NIFS spaxel flux density.

From Fig. 2, we can notice that the warm dust contribution fell rather sharply between 2011–2004 and 2013–2002, decreasing by a factor of 1.91 in the 0.3 arcsec data set. After that initial decrease, it falls within our error margin between 2013–2002 and 2015–2007 in the 0.3 arcsec data set, and then went down by a factor of 1.56 between 2015–2007 and 2021–2006. Since our spectra were taken roughly every 2 yr, any changes faster than this threshold would be

[1] 50 Myr, 100 Myr, 200 Myr, 500 Myr, 1 Gyr, 2 Gyr, 5 Gyr, 10 Gyr, and 15.8 Gyr.
[2] $Z = 0.00010$, 0.00152, 0.01914, and 0.02409.

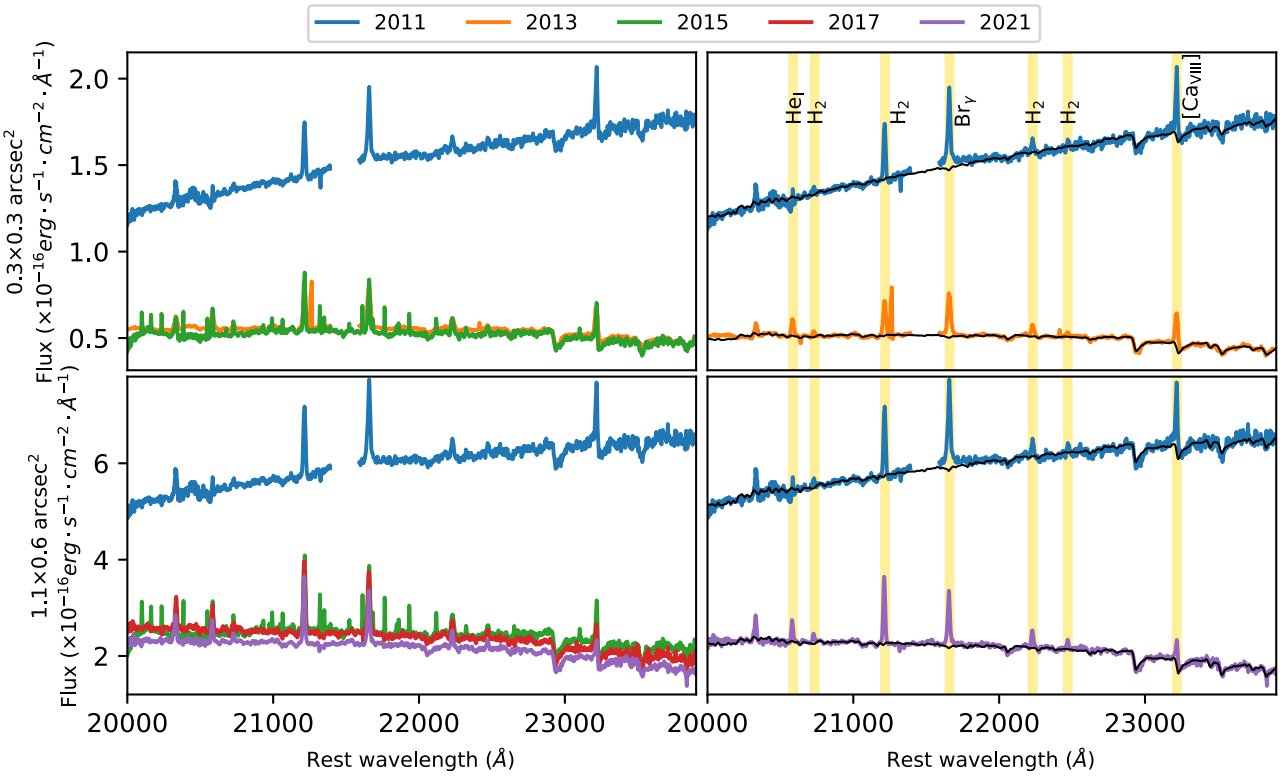

Figure 1. Spectra used in our analysis, where blue, orange, green, red, and purple represent those from yr 2011, 2013, 2015, 2017, and 2021, respectively. Left-hand panels show all spectra with the same aperture, whereas right-hand panels show only two, but with the modelled stellar population in black. At the right-hand panels, we also highlight in yellow the most prominent emission lines. Upper panels show spectra corresponding to an 0.3 arcsec × 0.3 arcsec extraction area, whereas bottom panels correspond to extractions of 1.1 arcsec × 0.6 arcsec.

Table 2. Continuum composition for spectra taken between 2011 and 2021 for the galaxy NGC 4388. These results correspond to percentage contribution or normalized flux at 22 780 Å.

Area	Date observed	FC (per cent)	BB_W (per cent)	BB_H (per cent)	StPop (per cent)	T_{BB} (K)	BB absolute flux (erg s^{-1} cm^{-2} Å^{-1})
0.3 arcsec × 0.3 arcsec	2011-04-12	0.	72.47	6.96	20.58	805 ± 112	1.19×10^{-16}
	2013-02-04	0.	37.87	0.	62.12	825 ± 118	2.07×10^{-17}
	2015-07-06	0.	35.92	0.	64.08	746 ± 49	1.90×10^{-17}
10 arcsec × 0.6 arcsec	2011-04-12	4.17	67.86	3.12	24.86	822 ± 124	4.27×10^{-16}
	2015-07-06	0.	36.41	0.	63.58	756 ± 49	8.95×10^{-17}
	2017-04-10	8.04	24.26	0.	67.7	873 ± 110	5.60×10^{-17}
	2021-06-28	0.	23.28	2.14	74.58	810 ± 104	4.88×10^{-17}

washed away in our analysis. However, this puts an upper limit of 2 ly (0.6 pc) at the size where this warm dust is located. This scale is compatible with the expected extent of the dusty torus (Zier & Biermann 2002).

For each epoch and data set, we estimated the median dust temperature by averaging the BB functions and weighting by luminosity. We found out that the BB temperature remained almost constant within the monitored period, inside our error margin. The average temperature for all observed epochs and data sets is 800 ± 100 K. According to Riffel et al. (2009), we can estimate the upper limit for the mass of the dust (M_{HD}) by

$$M_{HD} = \frac{4\pi}{3} a^3 N_{HD} \rho_{gr}, \quad (1)$$

where a is the grain radius, N_{HD} is the number of dust grains, and ρ_{gr} is the density of the grain. The number of dust grains can in turn be calculated as $N_{HD} = \frac{L_{ir}^{HD}}{L_{\nu,ir}^{gr}}$, where L_{ir}^{HD} is the total NIR luminosity due to dust, and $L_{\nu,ir}^{gr}$ is the infrared spectral luminosity of each dust grain.

Also, according to Riffel et al. (2009), the value of $L_{\nu,ir}^{gr}$ for a typical dust grain at 800 K is 15.08×10^{19} erg s^{-1} Hz^{-1}, the typical

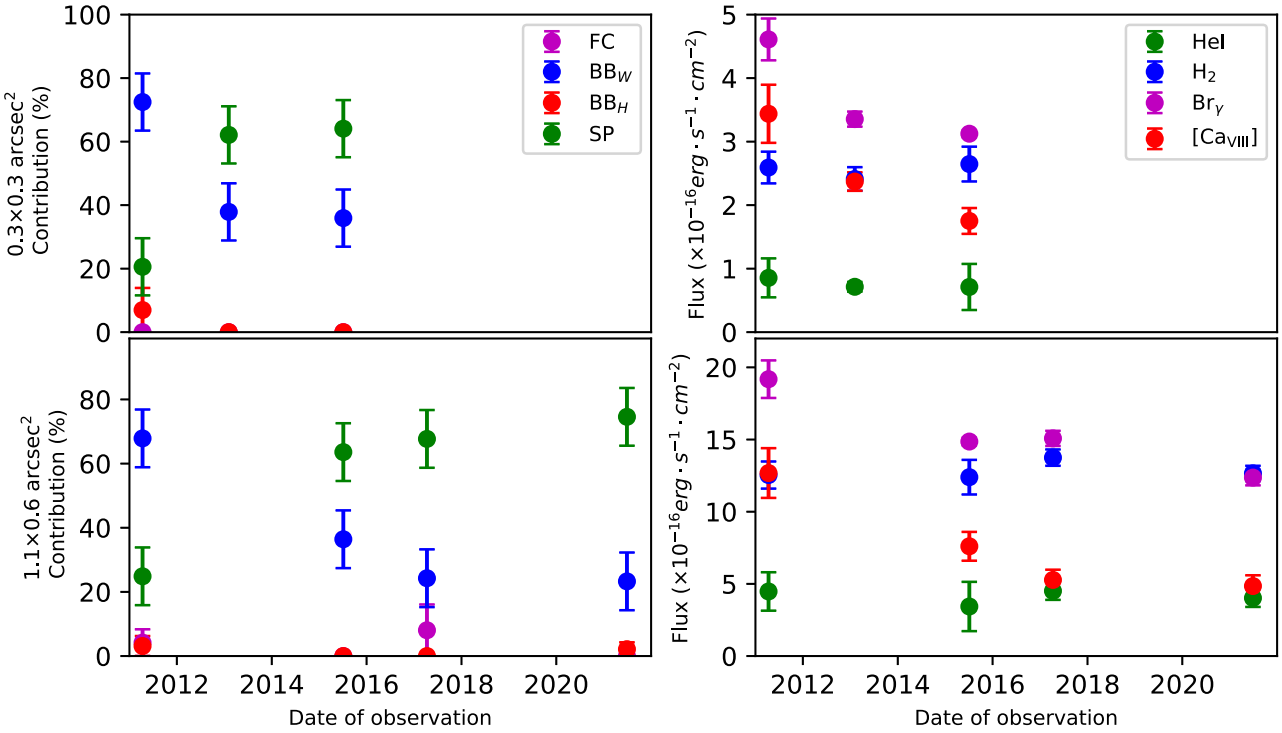

Figure 2. Left: Changes in continuum composition between 2011 and 2021 for NGC 4388, as estimated from STARLIGHT. Right: Variations in emission line fluxes in this same period, for the four most prominent lines. Upper panels show the result for our 0.3 arcsec data set and lower panels show the same results for our 0.6 arcsec data set.

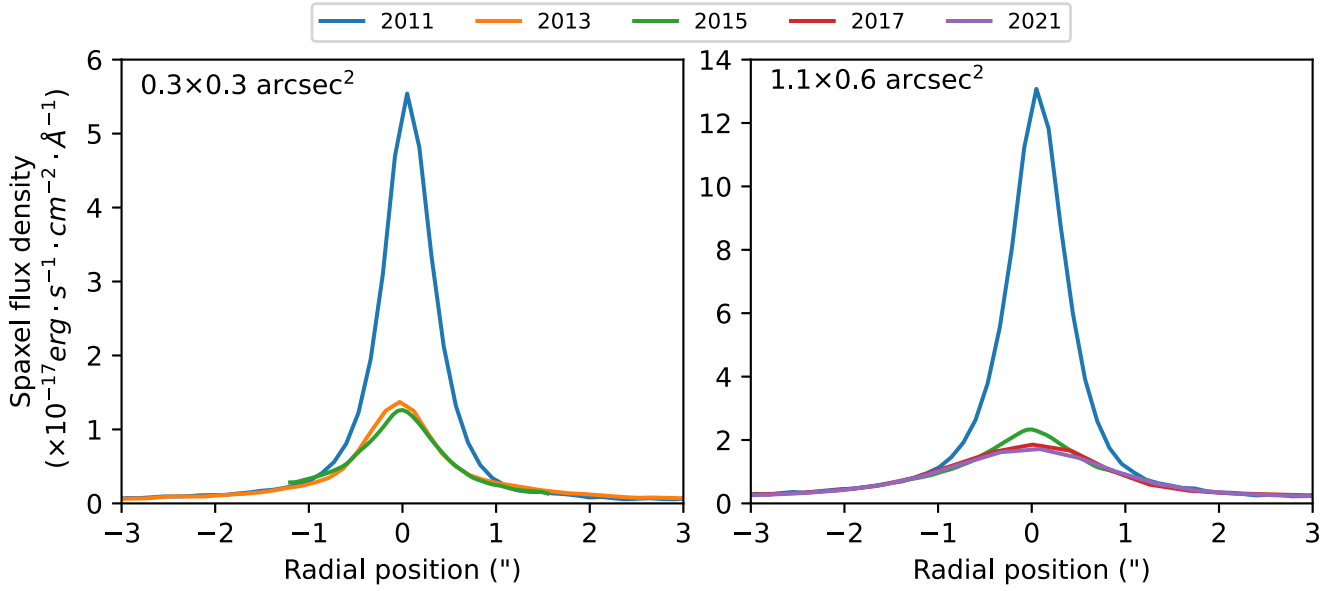

Figure 3. Comparison between the radial profile of the continuum for the five epochs, in both the 0.3 arcsec (left) and the 0.6 arcsec (right) sample. Since different data have different spaxel sizes, we normalized all data to the NIFS spaxel flux density.

density for graphite grains is 2.26 g cm^{-3}, and the typical grain radius is 0.05 μm (Granato & Danese 1994).

Thus, by integrating the NIR luminosity due to dust grains, we can see that the total warm dust was 8 × 10^{-3} M$_\odot$ in 2011, but has decreased to 0.9 × 10^{-3} M$_\odot$ in 2021. It means that this AGN had 88 per cent more warm dust grains in 2011 compared to 2021, but each dust grain emitted roughly the same energy.

4 EMISSION LINE VARIABILITY

We also tracked how the emission lines varied in this same period. We measured the fluxes of the four most prominent emission lines: He Iλ20587Å, H$_2$λ21218Å, Br γ and [Ca VIII]λ23211. We did this by first subtracting the continuum derived in Section 3, then measuring the zero flux level by selecting continuum bandpasses to the left and

Table 3. Emission line fluxes of the four most prominent emission lines in the *K* band. All fluxes and uncertainties are in units of 10^{-16} erg s^{-1} cm^{-2} Å^{-1}.

Area	Date observed	He I	H_2	Br γ	[Ca VIII]
03 arcsec × 03 arcsec	2011-04-12	0.85 ± 0.30	2.59 ± 0.25	4.61 ± 0.33	3.44 ± 0.45
	2013-02-04	0.71 ± 0.07	2.41 ± 0.18	3.35 ± 0.12	2.37 ± 0.14
	2015-07-06	0.71 ± 0.36	2.65 ± 0.27	3.12 ± 0.05	1.75 ± 0.20
1.1 arcsec × 0.6 arcsec	2011-04-12	4.47 ± 1.33	12.54 ± 0.94	19.18 ± 1.30	12.68 ± 1.72
	2015-07-06	3.43 ± 1.70	12.39 ± 1.20	14.86 ± 0.26	7.60 ± 0.99
	2017-04-10	4.51 ± 0.62	13.75 ± 0.56	15.08 ± 0.52	5.27 ± 0.70
	2021-06-28	4.02 ± 0.62	12.66 ± 0.52	12.36 ± 0.54	4.85 ± 0.74

right of the emission line, and finally integrating the area below the emission line. We notice a false emission feature close to H_2 in the GNIRS spectrum obtained in 2013. The spike is very close to the Gaussian profile fit to the molecular line. Thus, when performing the integration, we chose the limits for the emission line and its respective bandpasses aimed at avoiding this flaw. These emission line fluxes are presented in Table 3, and on the right-hand panel of Fig. 2.

Within the 10 yr monitored period, we detected no variation beyond our error margin in both He I and H_2. On the other hand, the atomic line fluxes of Br γ and [Ca VIII] decreased in the monitored period, 35 per cent and 61 per cent, respectively.

However, besides these changes being smaller than the 88 per cent warm dust variability in this same period, they were also slower. Between 2011–2004 and 2013–2002, Br γ and [Ca VIII] varied by 27 per cent and 31 per cent in the inner 0.3 arcsec × 0.3 arcsec, respectively. Normalizing that by the total per cent variation between 2011 and 2021 (derived from the 0.6 arcsec data set), this corresponds to ∼77 per cent and 49 per cent of the total variation in these 10 yr. On the other hand, in this same period the warm dust flux decreased by 93 per cent of the total variation in the monitored period. These results suggest that the warm dust in NGC 4388 is more internal than the region where Br γ and [Ca VIII] are produced. As can be seen in Table 3, most of the [Ca VIII] variation happened between 2011 and 2017, with the flux remaining almost constant after that. Although both ions show spatially resolved emission, which will be discussed in a future paper, our result shows that the bulk of the [Ca VIII] emission is produced in the inner 2 pc (∼6 ly), as opposed to 0.6 pc for the warm dust. While the warm dust emission is likely produced by the torus itself, either in its inner or its outer walls, [Ca VIII] is produced in a larger region, possibly in the direction of the ionization cone.

Br γ, on the other hand, still presented a variation of 18 per cent between 2017–2004 and 2021–2006, which means it is more extended than [Ca VIII], spanning a region bigger than 10 ly (∼3 pc). Lastly, the He I and H_2 are even more external, with the bulk of their emission being produced by the host galaxy (Rodríguez-Ardila, Riffel & Pastoriza 2005; Riffel et al. 2013), rather than the central source.

There are three differences between our work and the reverberation mapping studies of Landt et al. (2019, 2023): First, they aimed at Seyfert 1 galaxies, whereas we analysed an object where we cannot directly access the central source. Secondly, their estimated temperature for the dust in the nuclear region lies in the range 1000–1500 K. Lastly, they detected variations on time-scales of months, while we detected variations spanning one decade. Since our spectra were obtained roughly every 2 yr, we do not have enough information to rule out variabilities on shorter time-scales, and therefore all our results are upper limits to these time-scales and sizes. However, if variations on shorter time-scales were present, we would expect to observe more chaotic behaviour between different epochs, such as ups and downs and with varying amplitude. This is in contrast to the smooth variations detected in our analysis, with consistent amplitude and always in one direction. These key differences between our work and the previous reverberation studies in the NIR point to the fact that they were mapping a much more internal region, which is not accessible in NGC 4388. In their study, since the temperatures they derived are close to the one at which dust is expected to sublimate, such dust emission very likely comes from the inner walls of the torus, whereas the emission that we detected is more external than that, coming either from the middle or the outer walls of the torus.

Since this target has confirmed variability in X-rays (Fedorova et al. 2011), they are possibly causing the variations detected in our study. The X-ray variations have time-scales of 3–6 months, which means that they are produced in a region closer to the SMBH, no further than 0.15 pc from the central source. Although these time intervals point to smaller physical scales than the ones probed throughout this paper, according to Sanfrutos et al. (2016) they still track scales associated with the clumpy torus. Given the variability detected in the NIR and its probable association to the X-rays in NGC 4388, it will be very important to carry out a monitoring study in this object in both spectral regions. It will allow us to set firm constraints to the geometry of both emission regions.

It is worth noticing that we cannot rule out the possibility that these changes are caused by a clump of dust, partially obscuring the warm dust and the emission lines. Nonetheless, the time-scales of the variations put a hard constraint on the sizes of the regions detected throughout this paper, since even in the scenario of dust obscuration, the time necessary to eclipse a spectroscopic feature is directly linked to the size of such region.

5 FINAL REMARKS

We have monitored the Seyfert 1.9/2 galaxy by means of *K*-band spectroscopy over a period of 10 yr. To the best of our knowledge, it is the first time in the literature that an obscured AGN is monitored in that spectral region. The analysis has allowed us to detect variations in the warm dust emission, never before reported in that source, as well as to constrain the distance of the nuclear dust and the most prominent *K*-band emission lines in the inner 3 pc. Our main conclusions can be summarized as follows:

(i) The dust emission, which has an average temperature of 800 ± 100 K, decreased 88 per cent in flux during the monitoring period. Most of its variation occurred in the first 2 yr, which constrains

this emission to the inner 0.6 pc. This puts this emission at the scale of the torus, and since this temperature is much lower than the dust sublimation temperature, this emission likely comes from the middle or outer walls of the torus.

(ii) The emission lines of [Ca VIII] and Br γ also varied in this period. Whereas the coronal emission decreased 61 per cent, ionized hydrogen decreased 35 per cent. However, besides varying less than the warm dust, their variation also took longer. We were able to determine that the bulk of nuclear [Ca VIII] is produced in the inner 2 pc, with the Br γ associated to the central source spanning a region larger than 3 pc.

(iii) In the same period, we detected no variation of H_2 or He I beyond our error margin. This suggests that the emission from the AGN does not play a big role in these two lines, with most of their emission probably originating in the host galaxy.

Galaxies with variable properties are essential to aid us in constraining the properties of AGN, since the central source cannot be resolved by most telescopes. By adding NGC 4388 to the list of galaxies with confirmed NIR variability, we expect to assist disentangling the geometry of the inner unresolved region of AGNs.

ACKNOWLEDGEMENTS

We thank the anonymous referee for carefully reading the paper and providing suggestions that helped improving the quality of the manuscript. Supported by National Key R&D Program of China No.2022YFF0503402. ARA acknowledges financial support from Conselho Nacional de Desenvolvimento Científico e Tecnológico (Proj.). MB acknowledges funding support from programme JWST-GO-01717, which was provided by NASA through a grant from the Space Telescope Science Institute, which is operated by the Association of Universities for Research in Astronomy, Inc., under NASA contract NAS 5–03127. RR acknowledges support from the Fundación Jesús Serra and the Instituto de Astrofísica de Canarias under the Visiting Researcher Programme 2023–2025 agreed between both institutions. RR also acknowledges support from the ACIISI, Consejería de Economía, Conocimiento y Empleo del Gobierno de Canarias, and the European Regional Development Fund (ERDF) under grant with reference ProID2021010079, and the support through the RAVET project by the grant PID2019-107427GB-C32 from the Spanish Ministry of Science, Innovation and Universities MCIU. This work has also been supported through the IAC project TRACES, which is partially supported through the state budget and the regional budget of the Consejería de Economía, Industria, Comercio y Conocimiento of the Canary Islands Autonomous Community. RR also thanks Conselho Nacional de Desenvolvimento Científico e Tecnológico (CNPq, Proj. 311223/2020-6, 304927/2017-1 and 400352/2016-8), Fundação de amparo à pesquisa do Estado do Rio Grande do Sul (FAPERGS, Proj. 16/2551-0000251-7 and 19/1750-2), Coordenação de Aperfeiçoamento de Pessoal de Nível Superior (CAPES, Proj. 0001). RAR acknowledges financial support from Conselho Nacional de Desenvolvimento Científico e Tecnológico (Proj. 303450/2022-3) and Fundação de Amparo à pesquisa do Estado do Rio Grande do Sul (Proj. 21/2551-0002018-0).

DATA AVAILABILITY

All data used in this paper are publicly available, and can be freely downloaded through their respective telescope data archives.

REFERENCES

Bischetti M. et al., 2017, A&A, 598, A122
Bonnet H. et al., 2003, in Wizinowich P. L., Bonaccini D.eds, Proc. SPIE Conf. Ser. Vol. 4839, Adaptive Optical System Technologies II. SPIE, Bellingham, p. 329
Bressan A., Marigo P., Girardi L., Salasnich B., Dal Cero C., Rubele S., Nanni A., 2012, MNRAS, 427, 127
Burke C. J. et al., 2021, Science, 373, 789
Cackett E. M., Fabian A. C., Zogbhi A., Kara E., Reynolds C., Uttley P., 2013, ApJ, 764, L9
Cid Fernandes R., Gu Q., Melnick J., Terlevich E., Terlevich R., Kunth D., Rodrigues Lacerda R., Joguet B., 2004, MNRAS, 355, 273
Cid Fernandes R., Mateus A., Sodré L., Stasińska G., Gomes J. M., 2005, MNRAS, 358, 363
Cid Fernandes R. et al., 2014, A&A, 561, A130
Cushing M. C., Vacca W. D., Rayner J. T., 2004, PASP, 116, 362
Damas-Segovia A. et al., 2016, ApJ, 824, 30
Elias J. H., Rodgers B., Joyce R. R., Lazo M., Doppmann G., Winge C., Rodríguez-Ardila A., 2006a, in McLean I. S., Iye M.eds, Proc. SPIE Conf. Ser. Vol. 6269, Ground-based and Airborne Instrumentation for Astronomy. SPIE, Bellingham, p. 626914
Elias J. H., Joyce R. R., Liang M., Muller G. P., Hileman E. A., George J. R., 2006b, in McLean I. S., Iye M.eds, Proc. SPIE Conf. Ser. Vol. 6269, Ground-based and Airborne Instrumentation for Astronomy. SPIE, Bellingham, p. 62694C
Emmanoulopoulos D., Papadakis I. E., Dovčiak M., McHardy I. M., 2014, MNRAS, 439, 3931
Fedorova E. V., Beckmann V., Neronov A., Soldi S., 2011, MNRAS, 417, 1140
Forster K., Leighly K. M., Kay L. E., 1999, ApJ, 523, 521
Gaidos J. A. et al., 1996, Nature, 383, 319
Gaskell C. M., Klimek E. S., 2003, Astron. Astrophys. Trans., 22, 661
Granato G. L., Danese L., 1994, MNRAS, 268, 235
Hovatta T., Tornikoski M., Lainela M., Lehto H. J.,Valtaoja E., Torniainen I., Aller M. F., Aller H. D. , 2007, A&A, 469, 899
Hummel E., Saikia D. J., 1991, A&A, 249, 43
Koratkar A., Blaes O., 1999, PASP, 111, 1
Koshida S. et al., 2014, ApJ, 788, 159
Kroupa P., 2001, MNRAS, 322, 231
Kuo C. Y. et al., 2011, ApJ, 727, 20
Landt H. et al., 2019, MNRAS, 489, 1572
Landt H. et al., 2023, ApJ, 945, 62
McGregor P. J. et al., 2003, in Iye M., Moorwood A. F. M.eds, Proc. SPIEVol. 4841, Proc. SPIE Conf. Ser. Vol. 4841, Instrument Design and Performance for Optical/Infrared Ground-based Telescopes. SPIE, Bellingham, p. 1581
McHardy I. M., 2001, in Peterson B. M., Pogge R. W., Polidan R. S.eds, ASP Conf. Ser. Vol. 224, Probing the Physics of Active Galactic Nuclei. Astron. Soc. Pac., San Francisco, p. 205
McHardy I. M., Koerding E., Knigge C., Uttley P., Fender R. P., 2006, Nature, 444, 730
McHardy I. M. et al., 2014, MNRAS, 444, 1469
Marigo P., Bressan A., Nanni A., Girardi L., Pumo M. L., 2013, MNRAS, 434, 488
Mehdipour M. et al., 2017, A&A, 607, A28
Netzer H., 2015, ARA&A, 53, 365
Padovani P. et al., 2017, A&AR, 25, 2
Peterson B. M., 2001, in Aretxaga I., Kunth D., Mújica R.eds, Advanced Lectures on the Starburst-AGN Connection. World Scientific, Singapore, p. 3
Riffel R., Pastoriza M. G., Rodríguez-Ardila A., Bonatto C., 2009, MNRAS, 400, 273
Riffel R., Rodríguez-Ardila A., Aleman I., Brotherton M. S., Pastoriza M. G., Bonatto C., Dors O. L., 2013, MNRAS, 430, 2002
Riffel R. et al., 2022, MNRAS, 512, 3906
Rodríguez-Ardila A., Riffel R., Pastoriza M. G., 2005, MNRAS, 364, 1041

Rodríguez-Ardila A. et al., 2017, MNRAS, 465, 906
Sánchez P. et al., 2017, ApJ, 849, 110
Sanfrutos M., Miniutti G., Dovčiak M., Agís-González B., 2016, Astron. Nachr., 337, 546
Stone John L. J., Wilson A. S., Ward M. J., 1988, ApJ, 330, 105
Storchi-Bergmann T., Schnorr-Müller A., 2019, Nat. Astron., 3, 48
Vacca W. D., Cushing M. C., Rayner J. T., 2003, PASP, 115, 389
Veilleux S., Bland-Hawthorn J., Cecil G., 1999, AJ, 118, 2108
Verro K. et al., 2022, A&A, 661, A50
Vollmer B., Pappalardo C., Soida M., Lançon A., 2018, A&A, 620, A108
Winge C., Peterson B. M., Horne K., Pogge R. W., Pastoriza M. G., Storchi-Bergmann T., 1995, ApJ, 445, 680
Winge C., Peterson B. M., Pastoriza M. G., Storchi-Bergmann T., 1996, ApJ, 469, 648
Yoshida M. et al., 2002, ApJ, 567, 118
Zier C., Biermann P. L., 2002, A&A, 396, 91

This paper has been typeset from a TEX/LATEX file prepared by the author.